RSC Advances

PAPER

View Article Online
View Journal | View Issue

Cite this: *RSC Adv.*, 2025, **15**, 27661

High performance UiO-66 through microwave-assisted and Cr doping for adsorption heat storage applications

Guodong Fu,[a] Ping Wu, *[b] Jinguang Yang,[b] Shang Liu,[b] Shiping Zhang[b] and Xiulan Huai[c]

The metal–organic framework UiO-66 is a promising water vapor adsorbent due to its stability and hydrophilicity. In this study, we systematically investigated the modulation of pore structure and water adsorption performance of UiO-66 through microwave-assisted synthesis and controlled Cr^{3+} doping. The results indicated that the crystalline integrity and thermal stability of the framework remained well-preserved after doping. The UiO-66 samples with Cr^{3+} addition have higher pore volume and specific surface area. When the mole ratio of Cr to Zr is 1.5, the micropore volume and BET specific surface area of MW-1.5Cr-UiO-66 are 15.1% and 19.8% higher than MW-UiO-66. This structural optimization resulted in superior adsorption performance, with the saturated water adsorption capacity of MW-1.5Cr-UiO-66 reaching 0.59 g g^{-1}. Furthermore, the water adsorption capacity of MW-1.5Cr-UiO-66 remained unchanged after 10 cycles. The coordinated modulation of pore architecture and surface chemistry through transition metal doping provides new insights for developing high-performance adsorbents in adsorption heat storage applications.

Received 20th May 2025
Accepted 24th July 2025

DOI: 10.1039/d5ra03542b

rsc.li/rsc-advances

Introduction

In recent decades, humans have become increasingly eager to improve energy utilization efficiency and search for clean, renewable energy sources due to the depletion of fossil energy reserves, the rapid growth of energy consumption, and global environmental deterioration.[1,2] Adsorption heat storage is a type of thermochemical energy storage system that uses the adsorption/desorption process to achieve energy utilization.[3] It can effectively improve the energy grade and will not produce toxic and harmful substances. Therefore, it serves as an effective way to solve the problem of insufficient energy supply. Searching for suitable adsorbent–adsorbate working pairs is a standard method to improve the performance of the adsorption heat storage. Water is a promising adsorbate because of its non-toxicity, easy availability, and high latent heat of vaporization.[4]

Ideal adsorbent materials should possess three fundamental characteristics: high porosity, exceptional adsorption capacity, and robust cycling stability. In recent years, metal–organic frameworks (MOFs) are expected to be widely used in the fields of gas capture,[5–7] catalysis,[8–10] and medicine[11] due to their tunable architectures, ultrahigh surface areas, and tailorable pore environments. The studies of Canivet *et al.*[12] and Pritha *et al.*[13] demonstrated the excellent potential of MOFs as adsorbents for adsorption heat storage. Afterwards, researchers have shown increasing concern about the application of MOFs in the adsorption heat storage.

However, a critical limitation hinders their water-based applications: the inherent hydrolytic instability of metal–ligand coordination bonds.[14] Fortunately, pioneering work by DeCoste *et al.*[15] and Furukawa *et al.*[16] has revealed two key advantages of UiO-66: unparalleled chemical stability in aqueous environments and exceptional performance in water adsorption–desorption cycling tests. As a type of metal–organic framework with a face-centered cubic crystal structure, UiO-66 is composed of Zr_6O_4 $(OH)_4$ clusters and 1,4-benzoate (BDC) ligands.[17] Nevertheless, the low hydrophilicity and saturated water uptake (0.36 g g^{-1})[18] of UiO-66 limited its application in the field of adsorption heat storage.

Addressing these challenges, ligand functionalization strategies have proven effective in enhancing hydrophilicity. Notably, nitro- and amino-functionalized derivatives (UiO-66-NO_2 (ref. 19) and UiO-66-NH_2 (ref. 20)) demonstrate enhanced water vapor adsorption at reduced relative pressures compared to pure UiO-66. The water adsorption capacity of UiO-66 is primarily influenced by its specific surface area and microporous volume. This rationale has motivated metal doping approaches, where incorporating alien metal species into MOFs

[a]*School of Metallurgical and Ecological Engineering, Basic Experimental Center for Natural Science, University of Science and Technology Beijing, Beijing 100083, China*
[b]*Beijing Key Laboratory for Magneto-Photoelectrical Composite and Interface Science, School of Mathematics and Physics, University of Science and Technology Beijing, Beijing 100083, China. E-mail: pingwu@sas.ustb.edu.cn*
[c]*Institute of Engineering Thermophysics, Chinese Academy of Sciences, Beijing 100190, China*

can systematically enhance both surface areas and metal-active site densities,[21–23] critical factors for augmenting adsorption performance. For example, alkali metal (Li, K, and Na) doped MOF-5 have a higher specific surface area and excellent hydrogen adsorption performance compared with pure MOF-5.[21] Ebrahim *et al.*[22] found that the addition of Ce(III) increased the specific surface area and pore volume of the Zr-based metal–organic framework UiO-67 by 67% and 60%, respectively. Lau *et al.*[23] prepared a series of Ti-exchanged UiO-66 by the post-synthesis exchange method. When the ratio of Ti reaches 56%, the BET specific surface of UiO-66 (Ti_{56}) (1844 $m^2\ g^{-1}$) is 32.7% higher than pure UiO-66 (1390 $m^2\ g^{-1}$).

Collectively, these findings establish metal doping as a viable pathway for enhancing the adsorption capacity of UiO-66. The commonly used doping agents for UiO-66 modification include titanium, hafnium, and cerium.[21–23] These metal salts are generally expensive, and the synthesis steps of UiO-66 doped with these metals are relatively complex, posing particular risks. In contrast, chromium (Cr) salts are inexpensive and readily available. Building on these insights, we propose chromium doping combined with microwave-assisted hydrothermal (MAH) synthesis – an energy-efficient alternative to conventional hydrothermal methods that reduces reaction times from 24 hours to 2 hours (ref. 24) while minimizing energy consumption. In this study, a series of Cr-incorporated UiO-66 derivatives were systematically synthesized *via* MAH protocol. To elucidate the structure–function relationships, we have characterized the UiO-66 samples by scanning electron microscopy (SEM), X-ray diffraction (XRD), Fourier transform infrared spectroscopy (FT-IR), and N_2 adsorption tests. We have also studied the water vapor adsorption performances of Cr-modified UiO-66 by gravimetric adsorption.

Experimental section

Cr-doped UiO-66 was prepared by a microwave-assisted hydrothermal method. The following reagents were used: 1,4-benzene dicarboxylic acid (H_2BDC, 99%), *N*,*N*-dimethylformamide (DMF), hydrochloric acid (HCl), chromium nitrate nonahydrate ($Cr(NO_3)_3\cdot 9H_2O$, 99%), zirconium chloride ($ZrCl_4$, 99%), glacial acetic acid, and methanol. All chemicals were commercially sourced and used without further purification.

Synthesis of MW-*x*Cr-UiO-66

H_2BDC(0.476 g, 2.867 mmol), $ZrCl_4$(0.668 g, 2.867 mmol), and a certain amount of $Cr(NO_3)_3\cdot 9H_2O$ (0 g, 0.574 g, 1.147 g, 1.377, 1.721 g correspond to the molar ratio of Cr/Zr = 0, 0.5, 1.0, 1.2, 1.5 respectively) were dissolved in 45 mL of DMF. When a transparent solution was obtained, 5.0 mL of glacial acetic acid and 1.5 mL of HCl were added to the solution, and it was stirred continuously for 1 hour using a magnetic stirrer. The mixed solution was transferred to a 100 mL microwave reactor and maintained at 120 °C for 2 hours. The precipitates were centrifuged at 4000 rpm and washed three times with DMF and methanol, respectively. Then, the products were dried at 70 °C for 8 hours. Finally, the samples were heated under vacuum at 250 °C for 2 hours to remove the nitrate ions. According to the molar ratio x of $Cr(NO_3)_3\cdot 9H_2O$ to $ZrCl_4$, the samples were named MW-UiO-66 ($x = 0$) and MW-*x*Cr-UiO-66 ($x = 0.5, 1.0, 1.2, 1.5$).

Results and discussion

Surface morphology

A Zeiss field emission scanning electron microscope (SUPRA 55 SAPPHIRE) was used to study the effect of Cr^{3+} addition on the morphology of UiO-66 samples. The samples were coated with gold before the tests. As shown in Fig. 1, the crystal morphology of all samples is characterized by octahedral crystals with uneven crystal size distribution and agglomeration. Notably, progressive refinement in crystallite dimensions was observed with increasing Cr/Zr molar ratios. The statistical results of Nano Measurer showed that the average particle size of MW-UiO-66 is approximately 270 nm, whereas it is only about 210 nm for MW-1.5Cr-UiO-66.

Microstructures

The crystal structure of these samples was characterized by an X-ray diffractometer (XRD, Rigaku D/max2500X). The Cu K_α ray ($\lambda = 1.54056$ Å) (40 kV, 200 mA) was used as the X-ray source, and the selected 2θ scanning range was 5°–50° with a step of 0.01°. The XRD patterns are shown in Fig. 2. The XRD pattern of MW-UiO-66 revealed three dominating peaks at 7.4°, 8.5°, and 25.8°, corresponding to (111), (200), and (600) crystal planes, respectively.[25] The characteristic peaks of Cr-doped UiO-66 samples match well with MW-UiO-66, indicating that the presence of chromium will not affect the formation of the crystal structure of UiO-66.

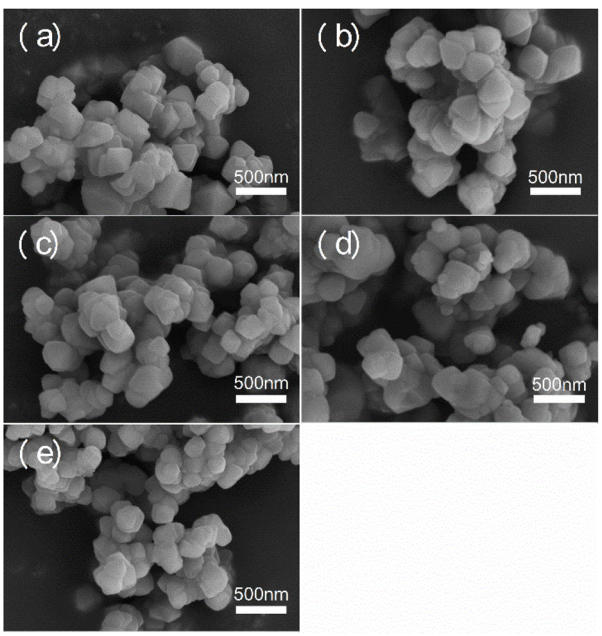

Fig. 1 SEM images of (a) MW-UiO-66, (b) MW-0.5Cr-UiO-66, (c) MW-1.0Cr-UiO-66, (d) MW-1.2Cr-UiO-66, (e) MW-1.5Cr-UiO-66.

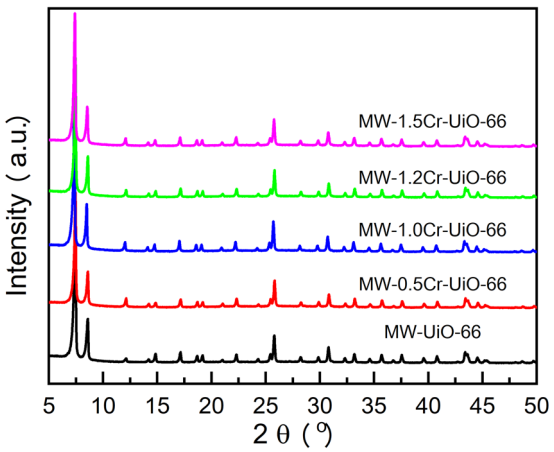

Fig. 2 XRD patterns of MW-*x*Cr-UiO-66 samples with different additions of Cr^{3+} (molar ratio Cr: Zr = 0, 0.5, 1.0, 1.2, 1.5).

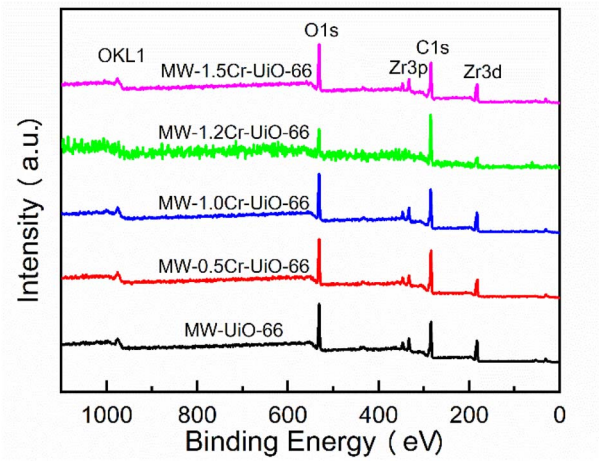

Fig. 4 XPS spectra of MW-*x*Cr-UiO-66 samples with different additions of Cr^{3+} (molar ratio Cr: Zr = 0, 0.5, 1.0, 1.2, 1.5).

The infrared spectrums of the samples in the range of 400–4000 cm^{-1} were measured using a Lambda FTIR-7600 Fourier transform infrared spectrometer. As shown in Fig. 3, two strong bands at 1578 and 1400 cm^{-1} are related to the asymmetric and symmetric stretching vibrations of the OCO group in the carboxylic acid group, respectively.[26] The small band at 1508 cm^{-1} corresponds to the vibration of the C=C double bond in the benzene ring. The bands at 746 and 665 cm^{-1} correspond to O–H and C–H vibration modes, respectively.[17,27] The infrared spectra of MW-*x*Cr-UiO-66 were similar to those of MW-UiO-66, and no additional absorption peak was observed. The spectral congruence between pristine and Cr-doped MOFs, coupled with no discernible coordination shifts, further corroborates XRD conclusions that the addition of Cr^{3+} did not change the crystal structure of UiO-66.

X-ray photoelectron spectroscopy (XPS) analysis was performed using a Thermo Scientific EscalabXi+ A9951381 equipment. As shown in Fig. 4, the spectra of MW-UiO-66 and MW-Cr-UiO-66 samples are similar. All samples did not exhibit any new characteristic peaks, indicating that only a small amount, or even no Cr^{3+}, was present in the framework of UiO-66. This may be due to the presence of acetic acid and hydrochloric acid interfering with the binding of Cr^{3+} to the BDC ligands, as well as the relatively short reaction time (only 2 hours).

Thermal stability

Thermogravimetric analysis (TGA) was performed on a synchronous thermal analyzer (PerkinElmer STA 8000) at a heating rate of 10 °C min^{-1}. As shown in Fig. 5, all samples exhibit high thermal stability and similar continuous weightlessness, which encompasses three main weightlessness stages. This is consistent with the report of Hu *et al.*[25] The first stage of weightlessness occurs between 30–200 °C, which is due to the evaporation of the water physically adsorbed in the cavities. The second weight-loss stage occurred between 200–350 °C, mainly due to the dehydroxylation of Zr–O clusters in the framework of UiO-66.[28] The third weight-loss stage begins at 450 °C, and the

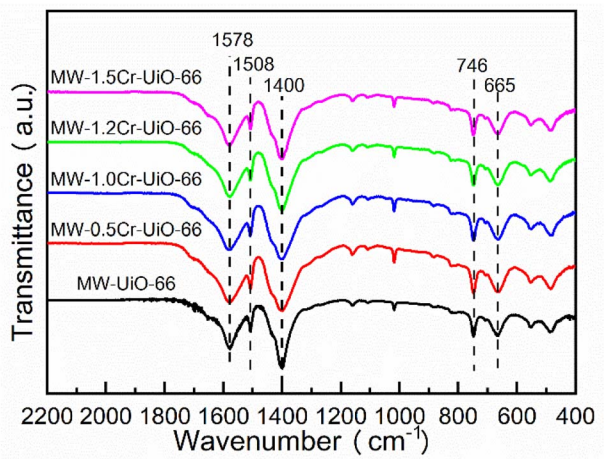

Fig. 3 FTIR curves of MW-*x*Cr-UiO-66 samples with different additions of Cr^{3+} (molar ratio Cr: Zr = 0, 0.5, 1.0, 1.2, 1.5).

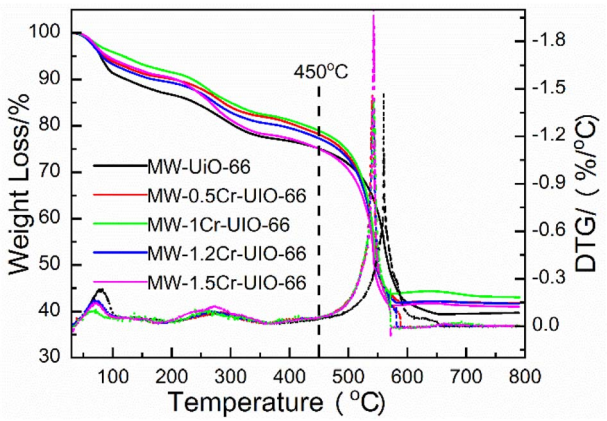

Fig. 5 TG and DTG curves of MW-*x*Cr-UiO-66 samples with different additions of Cr^{3+} (molar ratio Cr: Zr = 0, 0.5, 1.0, 1.2, 1.5).

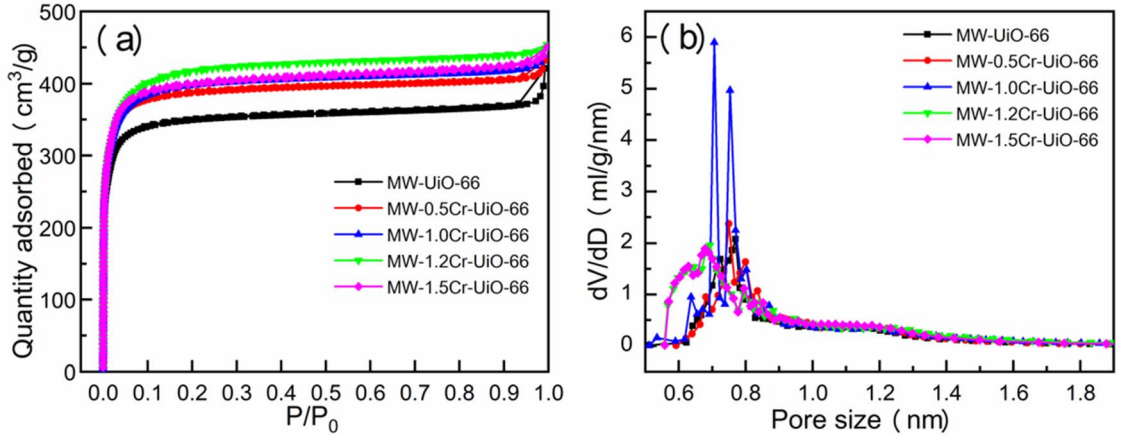

Fig. 6 Nitrogen sorption isotherms (a) and pore size distributions (b) of MW-*x*Cr-UiO-66 samples with different additions of Cr^{3+} (molar ratio Cr: Zr = 0, 0.5, 1.0, 1.2, 1.5).

skeleton structure of the samples decomposes and collapses at this temperature. Finally, only metallic oxides remained.

Shearer *et al.*[29] have proposed a method for the quantitative analysis of ligand defects in UiO-66 based on the weight-loss ratio. According to this method,[26] the weight loss of all samples is lower than that of defect-free UiO-66 (54.6%) between 450–700 °C, indicating that all samples are defective. As shown in Fig. 5, the weight loss of the samples with Cr^{3+} addition is lower than that of MW-UiO-66, indicating that the addition of Cr^{3+} may enhance the structural defects of MW-UiO-66.

Porosity

The nitrogen sorption isotherms were measured using a nitrogen adsorption–desorption tester (Beishide 3H-2000PM) at 77 K to obtain pore structure information of the samples. Before the tests, the samples were activated under vacuum at 150 °C for 4 hours. As shown in Fig. 6(a), the nitrogen adsorption quantity of the samples increases rapidly to a high value at low relative pressures. Then, the isotherms almost show a horizontal platform after 0.2 P/P_0 and have a "tailing" at saturation pressure. These are typical characteristics of type I sorption isotherms, indicating that all samples have typical microporous structures. With the increase in the Cr to Zr ratio, the nitrogen adsorption capacity increased gradually, indicating that the porosity of the samples also increased.

The pore size distributions obtained by Horvath–Kawazoe (H–K) model analysis are presented in Fig. 6(b). Combined with Table 1, the pore size of the sample decreases gradually with increasing Cr addition, while the specific surface area and pore volume increase. The BET-specific surface area of MW-1.5Cr-UiO-66 (1524 $m^2\ g^{-1}$) is 19.8% higher than the unmodified MW-UiO-66 (1272 $m^2\ g^{-1}$). These results suggest an increase in structural defects resulting from the addition of Cr, which is beneficial for enhancing the adsorption capacity of the samples.

Adsorption properties

The isotherms of water vapor adsorption were measured on a multi-station steam adsorption instrument (Beishide 3H-2000PM) at 25 °C. As shown in Fig. 7, the sorption isotherms of all samples exhibit similar "*S*" adsorption curves, indicating a consistent adsorption mechanism for water vapor. The water vapor adsorption quantity of the samples increases sharply at $0.2 < P/P_0 < 0.5$. The water vapor uptake of the samples is close to saturation at $P/P_0 = 0.5$, and the subsequent increase may be due to the adsorption of water into the voids between grains.[30] With the increase of Cr^{3+} addition, the saturated water vapor adsorption capacity of the samples increased gradually from 0.54 g/g (MW-UiO-66) to 0.59 g/g (MW-1.5Cr-UiO-66).

The water vapor adsorption mechanism of porous materials mainly depends on the pore size distribution. According to the studies of Canivet *et al.*,[12] when the pore diameter of the material is smaller than the critical size D_C (D_C = 2.0 nm for water), water clusters form within the material instead of capillary condensation. Therefore, it is a water cluster

Table 1 Pore structure information of MW-*x*Cr-UiO-66 samples with different additions of Cr^{3+} (molar ratio Cr: Zr = 0, 0.5, 1.0, 1.2, 1.5)

Sample	S_{BET} ($m^2\ g^{-1}$)	V_{Micro} ($cm^3\ g^{-1}$)	V_{Total} ($cm^3\ g^{-1}$)	Water uptake at P/P_0 = 0.9 (g/g)
MW-UiO-66	1272	0.53	0.65	0.54
MW-0.5Cr-UiO-66	1454	0.59	0.67	0.57
MW-1.0Cr-UiO-66	1422	0.60	0.68	0.58
MW-1.2Cr-UiO-66	1487	0.63	0.70	0.57
MW-1.5Cr-UiO-66	1524	0.61	0.70	0.59

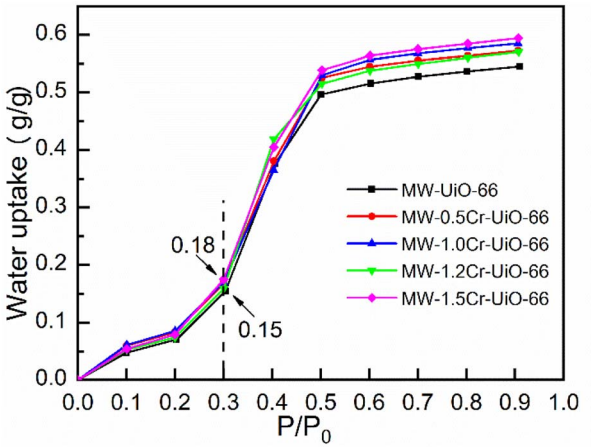

Fig. 7 Water vapor sorption isotherms of MW-*x*Cr-UiO-66 samples with different additions of Cr^{3+} (molar ratio Cr: Zr = 0, 0.5, 1.0, 1.2, 1.5).

adsorption process for UiO-66 due to the micropore size of 0.5–1.0 nm. Compared with MW-UiO-66, the micropore volume of MW-1.5Cr-UiO-66 increased by 15.1%. Fig. 6(b) shows that the newly generated pore is mainly distributed in the size range of 0.55–0.65 nm, which is only slightly larger than the effective diameter of a water molecule (0.28 nm). Narrow pores are not conducive to the diffusion and adsorption of water molecules in UiO-66, resulting in a lower increase in saturated water vapor adsorption capacity (9.3%) for MW-1.5Cr-UiO-66. The cyclic stability of MW-UiO-66 and MW-1.5Cr-UiO-66 was tested, and the results are shown in Fig. 8. At 25 °C and 30% relative humidity, the initial water adsorption capacity of MW-UiO-66 and MW-1.5Cr-UiO-66 reached 0.38 g/g and 0.40 g/g, respectively. The water adsorption capacity of MW-UiO-66 decreased by 5.3% after 10 cycles, while the water adsorption capacity of MW-1.5Cr-UiO-66 remained unchanged after 10 cycles, demonstrating good stability.

Compared with the Zr-based MOF materials in some literature,[18–20,31–34] the water vapor adsorption capacity of MW-1.5Cr-UiO-66 is relatively high (Table 2), which is more conducive to the application of UiO-66 in the field of adsorption heat storage. The BET surface area of the 0.5Cr-UiO-66 synthesized by the solvothermal method is smaller than Ce-UiO-66 and $Al_{0.3}Zr_{0.7}$-UiO-66. This indicates that the process of Cr doping synthesized by solvothermal cannot significantly improve the pore structure and specific surface area of UiO-66. But with the addition of hydrochloric acid and acetic acid as regulators, the microwave-assisted Cr-doped UiO-66 sample showed significant improvements in water uptake and specific surface area. Moreover, this methodology enhanced thermal stability, with microwave-derived samples maintaining structural integrity up to 450 °C, surpassing the 400 °C stability limit observed in solvothermally prepared Cr-doped UiO-66.[34]

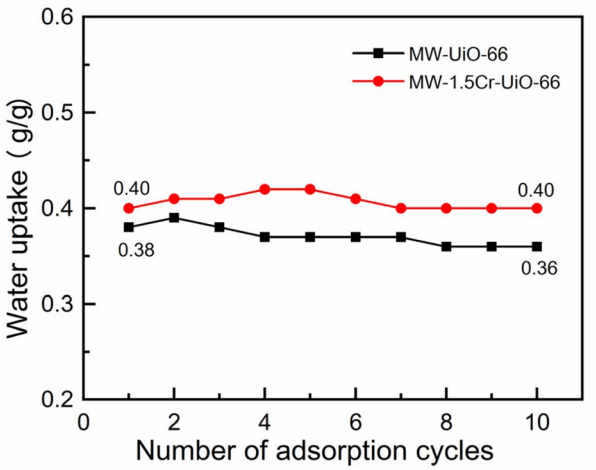

Fig. 8 Water adsorption cycles of MW-UiO-66 and MW-1.5Cr-UiO-66.

Table 2 Water vapor adsorption capacities of some reported Zr-based MOFs measured at 298 K

MOF	S_{BET} ($m^2\ g^{-1}$)	Water vapor uptake (g/g)	Ref.
UiO-66	1030	0.36	18
UiO-66-NO_2	792	0.37	19
UiO-66-NH_2	1093	0.37	20
Ce-UiO-66	1120	—	31
Mn-UiO-66	797	—	32
$Al_{0.3}Zr_{0.7}$-UiO-66	1060	—	33
0.5Cr-UiO-66	946	0.50	Previous work[34]
MW-1.5Cr-UiO-66	1524	0.59	This paper

As a typical microporous material, the adsorption performance of UiO-66 is mainly affected by the pore structure and chemical environment. Previous studies[21–23] have shown that incorporating alien metal species into MOFs can effectively enhance both surface areas and active site densities, critical factors for augmenting adsorption performance. In this study, the results of SEM showed that the crystal size decreased as the amount of $Cr(NO_3)_3 \cdot 9H_2O$ added increased. This phenomenon suggests that the addition of Cr^{3+} interferes with or inhibits the growth of UiO-66 grains by affecting the binding of Zr^{4+} to BDC ligands,[34] thereby increasing the probability of defects or incorrect coordination in the UiO-66 structure. The BET surface area of MW-1.5Cr-UiO-66 is 19.8% higher than that of MW-UiO-66, confirming that MW-1.5Cr-UiO-66 has higher defects or incorrect coordination.

However, the results of FTIR and XPS showed that the Cr doped UiO-66 samples did not exhibit any new characteristic peaks, indicating that only a small amount or even no Cr^{3+} was present in the framework of UiO-66. This may be due to the presence of acetic acid and hydrochloric acid[35] interfering with the binding of Cr^{3+} to the BDC ligands, and the relatively short reaction time (only 2 hours). In conclusion, the addition of $Cr(NO_3)_3 \cdot 9H_2O$ will lead to more defects and mismatches in the UiO-66 structure, exposing more hydrophilic sites and thereby improving its hydrophilicity. The increased pore volume and specific surface area result in a higher saturation water adsorption capacity of UiO-66.

Conclusions

In this paper, a series of samples of MW-*x*Cr-UiO-66 samples was prepared using a microwave-assisted hydrothermal method. Systematic characterization revealed that the addition of Cr^{3+} can improve the specific surface area and water vapor adsorption capacity of UiO-66. MW-1.5Cr-UiO-66 has the highest BET specific surface area (1524 m^2 g^{-1}) and water vapor adsorption capacity (0.59 g/g). And the water adsorption capacity of MW-1.5Cr-UiO-66 remained unchanged after 10 cycles. The crystal structure of UiO-66 remained unchanged by the addition of Cr^{3+}, and all samples retained high thermal stability. The structural modification, attributed to controlled defect engineering through metal substitution, resulted in a 15.1% increase in micropore volume relative to unmodified UiO-66. This increase was beneficial for enhancing the adsorption capacity. These results may provide a basis for considering the application of UiO-66 material in the field of adsorption heat storage.

Conflicts of interest

There are no conflicts to declare.

Data availability

The data used to support the finding of this study was included within the manuscript.

Acknowledgements

This work was supported by the Fundamental Research Funds for the Central Universities (FRF-TP-25-088).

References

1 K. Dong, X. Dong and Q. Jiang, How renewable energy consumption lower global CO_2 emissions: Evidence from countries with different income levels, *World Econ.*, 2019, **43**, 1665–1698.
2 K. R. Abbasi, M. Shahbaz, J. Zhang, M. Irfan and R. Alvarado, Analyze the environmental sustainability factors of China: The role of fossil fuel energy and renewable energy, *Renew. Energy*, 2022, **187**, 390–402.
3 V. Palomba and A. Frazzica, Recent advancements in sorption technology for solar thermal energy storage applications, *Sol. Energy*, 2019, **192**, 69–105.
4 A. Rezk, A. Olabi, A. Alami, A. Radwan, H. Demir, S. Rahman, S. Shah and M. Abdelkareem, Experimental Study on Utilizing Silica Gel with Ethanol and Water for Adsorption Heat Storage, *Energies*, 2022, **16**, 444.
5 J. B. DeCoste, T. J. Demasky, M. J. Katz, O. K. Farha and J. T. Hupp, A UiO-66 analogue with uncoordinated carboxylic acids for the broad-spectrum removal of toxic chemicals, *New J. Chem.*, 2015, **39**, 2396–2399.
6 H.-Q. Yin, Z.-M. Zhang and T.-B. Lu, Ordered Integration and Heterogenization of Catalysts and Photosensitizers in Metal–/Covalent–Organic Frameworks for Boosting CO_2 Photoreduction, *Acc. Chem. Res.*, 2023, **56**, 2676–2687.
7 G. Zheng, K. Wei, X. Kang, W. Fan, N. L. Ma, M. Verma, H. S. Ng and S. Ge, A new attempt to control volatile organic compounds (VOCs) pollution – Modification technology of biomass for adsorption of VOCs gas, *Environ. Pollut.*, 2023, **336**, 122451.
8 K. Leus, P. Concepcion, M. Vandichel, M. Meledina, A. Grirrane, D. Esquivel, S. Turner, D. Poelman, M. Waroquier, V. Van Speybroeck, G. Van Tendeloo, H. García and P. Van Der Voort, Au@UiO-66: a base free oxidation catalyst, *RSC Adv.*, 2015, **5**, 22334–22342.
9 J. L. Obeso, J. G. Flores, C. V. Flores, M. T. Huxley, J. A. de los Reyes, R. A. Peralta, I. A. Ibarra and C. Leyva, MOF-based catalysts: insights into the chemical transformation of greenhouse and toxic gases, *Chem. Commun.*, 2023, **59**, 10226–10242.
10 X.-C. Yi, F.-G. Xi, Y. Qi and E.-Q. Gao, Synthesis and click modification of an azido-functionalized Zr(iv) metal-organic framework and a catalytic study, *RSC Adv.*, 2015, **5**, 893–900.
11 T. Kundu, S. Mitra, P. Patra, A. Goswami, D. Diaz Diaz and R. Banerjee, Mechanical downsizing of a gadolinium(III)-based metal-organic framework for anticancer drug delivery, *Chemistry*, 2014, **20**, 10514–10518.
12 J. Canivet, A. Fateeva, Y. Guo, B. Coasne and D. Farrusseng, Water adsorption in MOFs: fundamentals and applications, *Chem. Soc. Rev.*, 2014, **43**, 5594–5617.
13 P. Ghosh, Y. J. Colon and R. Q. Snurr, Water adsorption in UiO-66: the importance of defects, *Chem. Commun.*, 2014, **50**, 11329–11331.
14 X. Xia, M. Cao, Z. Liu, W. Li and S. Li, Elucidation of adsorption cooling characteristics of Zr-MOFs: Effects of structure property and working fluids, *Chem. Eng. Sci.*, 2019, **204**, 48–58.
15 J. B. DeCoste, G. W. Peterson, B. J. Schindler, K. L. Killops, M. A. Browe and J. J. Mahle, The effect of water adsorption on the structure of the carboxylate containing metal-organic frameworks Cu-BTC, Mg-MOF-74, and UiO-66, *J. Mater. Chem. A*, 2013, **1**, 11922.
16 H. Furukawa, F. Gandara, Y. B. Zhang, J. Jiang, W. L. Queen, M. R. Hudson and O. M. Yaghi, Water adsorption in porous metal–organic frameworks and related materials, *J. Am. Chem. Soc.*, 2014, **136**, 4369–4381.
17 J. H. Cavka, S. Jakobsen, U. Olsbye, N. Guillou, C. Lamberti, S. Bordiga and K. P. Lillerud, A New Zirconium Inorganic Building Brick Forming Metal Organic Frameworks with Exceptional Stability, *J. Am. Chem. Soc.*, 2008, **130**, 13850–13851.
18 J. Canivet, J. Bonnefoy, C. Daniel, A. Legrand, B. Coasne and D. Farrusseng, Structure-property relationships of water adsorption in metal–organic frameworks, *New J. Chem.*, 2014, **38**, 3102–3111.
19 G. E. Cmarik, M. Kim, S. M. Cohen and K. S. Walton, Tuning the adsorption properties of UiO-66 *via* ligand functionalization, *Langmuir*, 2012, **28**, 15606–15613.

20 H. J. An, M. Sarker, D. K. Yoo and S. H. Jhung, Water adsorption/desorption over metal-organic frameworks with ammonium group for possible application in adsorption heat transformation, *Chem. Eng. J.*, 2019, **373**, 1064–1071.
21 C.-L. Chu, J.-R. Chen and T.-Y. Lee, Enhancement of hydrogen adsorption by alkali-metal cation doping of metal–organic framework-5, *Int. J. Hydrogen Energy*, 2012, **37**, 6721–6726.
22 A. M. Ebrahim and T. J. Bandosz, Ce(III) doped Zr-based MOFs as excellent NO_2 adsorbents at ambient conditions, *ACS Appl. Mater. Interfaces*, 2013, **5**, 10565–10573.
23 C. H. Lau, R. Babarao and M. R. Hill, A route to drastic increase of CO_2 uptake in Zr metal organic framework UiO-66, *Chem. Commun.*, 2013, **49**, 3634–3636.
24 Y. Li, Y. Liu, W. Gao, L. Zhang, W. Liu, J. Lu, Z. Wang and Y.-J. Deng, Microwave-assisted synthesis of UIO-66 and its adsorption performance towards dyes, *CrystEngComm*, 2014, **16**, 7037–7042.
25 Z. Hu, Y. Peng, Z. Kang, Y. Qian and D. Zhao, A Modulated Hydrothermal (MHT) Approach for the Facile Synthesis of UiO-66-Type MOFs, *Inorg. Chem.*, 2015, **54**, 4862–4868.
26 L. Valenzano, B. Civalleri, S. Chavan, S. Bordiga, M. H. Nilsen, S. Jakobsen, K. P. Lillerud and C. Lamberti, Disclosing the Complex Structure of UiO-66 Metal Organic Framework: A Synergic Combination of Experiment and Theory, *Chem. Mater.*, 2011, **23**, 1700–1718.
27 Y. Cao, Y. Zhao, Z. Lv, F. Song and Q. Zhong, Preparation and enhanced CO_2 adsorption capacity of UiO-66/graphene oxide composites, *J. Ind. Eng. Chem.*, 2015, **27**, 102–107.
28 H. Wu, Y. S. Chua, V. Krungleviciute, M. Tyagi, P. Chen, T. Yildirim and W. Zhou, Unusual and Highly Tunable Missing-Linker Defects in Zirconium Metal–Organic Framework UiO-66 and Their Important Effects on Gas Adsorption, *J. Am. Chem. Soc.*, 2013, **135**, 10525–10532.
29 G. C. Shearer, S. Chavan, S. Bordiga, S. Svelle, U. Olsbye and K. P. Lillerud, Defect Engineering: Tuning the Porosity and Composition of the Metal–Organic Framework UiO-66 *via* Modulated Synthesis, *Chem. Mater.*, 2016, **28**, 3749–3761.
30 P. Küsgens, M. Rose, I. Senkovska, H. Fröde, A. Henschel, S. Siegle and S. Kaskel, Characterization of metal-organic frameworks by water adsorption, *Microporous Mesoporous Mater.*, 2009, **120**, 325–330.
31 X. Du, S. Feng, J. Luo, Y. Zhuang, W. Song, X. Li and Y. Wan, Pebax mixed matrix membrane with bimetallic CeZr-MOFs to enhance CO_2 separation, *Sep. Purif. Technol.*, 2023, **322**, 124251.
32 Z.-h. Yang, J. Cao, Y.-p. Chen, X. Li, W.-p. Xiong, Y.-y. Zhou, C.-y. Zhou, R. Xu and Y.-r. Zhang, Mn-doped zirconium metal–organic framework as an effective adsorbent for removal of tetracycline and Cr(VI) from aqueous solution, *Microporous Mesoporous Mater.*, 2019, **277**, 277–285.
33 P. Liu, J. Lyu and P. Bai, One-Step Synthesis of Al-Doped UiO-66 Nanoparticle for Enhanced Removal of Organic Dyes from Wastewater, *Molecules*, 2023, **28**, 2182.
34 G. Fu, P. Wu, J. Yang, S. Zhang and X. Huai, Cr-doped UiO-66 with enhanced water adsorption for adsorption heat transformation, *Microporous Mesoporous Mater.*, 2022, **331**, 111642.
35 W. Liang, C. J. Coghlan, F. Ragon, M. Rubio-Martinez, D. M. D'Alessandro and R. Babarao, Defect engineering of UiO-66 for CO_2 and H_2O uptake – a combined experimental and simulation study, *Dalton Trans.*, 2016, **45**(11), 4496–4500.